nature biotechnology

Article

https://doi.org/10.1038/s41587-026-03081-9

# Artificial allosteric protein switches with machine-learning-designed receptors

Received: 30 September 2025

Accepted: 9 March 2026

Published online: 15 April 2026

Check for updates

Zhong Guo[1,2,3], Oleh Smutok[4], Gyu Rie Lee[5,6,7,15], Zhenling Cui[1,2,3,8], Haocheng Qianzhu[9], Monika Kish[10], Cagla Ergun yva[1,2,3], Kejia Wu[5,6,7], Roxane Mutschler[1,2,3], Colin J. Jackson[1,9,11], Maria M. Fiorito[1,2,3], Andrew C. Warden[12], Oliver B. Smith[1,9], Alfredo Quijano-Rubio[13], Thomas Huber[9], Jonathan J. Phillips[10,14], Gottfried Otting[11], Evgeny Katz[4], David Baker[5,6,7] & Kirill Alexandrov[1,2,3]

Protein allostery underlies most information and energy processing in biology and the development of artificial allosteric proteins is a key objective of synthetic biology and biotechnology. We show that machine-learning-engineered minimal ligand-binding domains act as efficient receptors in single-component allosteric switches, despite lacking global conformational change. Such colorimetric, luminescent and electrochemical biosensors of small molecules, peptides and proteins can be compiled into intramolecular YES and AND logic gates. Furthermore, we report fully synthetic allosteric switches composed of artificial receptor and reporter domains. Hydrogen/deuterium exchange mass spectrometry and $^{19}$F nuclear magnetic resonance analyses suggest that ligand binding reduces the conformation entropy of the system, increasing the catalytic activity of the reporter domain. The potential practical utility of this approach is demonstrated by engineering *Escherichia coli* cells with steroid-dependent antibiotic resistance and by developing bioelectronic devices capable of quantifying steroid hormones.

Almost all real-time biological information and energy processing occurs within protein networks composed of protein switches. These networks are governed by protein allostery, whereby a local input generates a response at a distant functional site[1]. Therefore, construction of artificial allosteric protein systems with inputs and outputs of choice is a central objective of protein engineering and synthetic biology. Artificial fluorescent protein switches (biosensors) have transformed cell and neurobiology by revealing real-time concentration changes in calcium, neurotransmitters and other small molecules in cells and organisms[2]. Such switches are typically composed of a ligand-binding domain inserted into a fluorescent protein reporter. Ligand-binding domains have traditionally been chosen on the basis of ligand specificity, affinity and a ligand-induced macromolecular conformation change. Similar approaches have been used to develop chimeras between ligand-binding domains and enzymatic reporters such as proteases, carbohydrate dehydrogenases, β-lactamases and luciferases[3–8].

[1]ARC Centre of Excellence in Synthetic Biology, Brisbane, Queensland, Australia. [2]Centre for Agriculture and the Bioeconomy, Queensland University of Technology, Brisbane, Queensland, Australia. [3]School of Biology and Environmental Science, Queensland University of Technology, Brisbane, Queensland, Australia. [4]Department of Chemistry and Biochemistry, Clarkson University, Potsdam, NY, USA. [5]Department of Biochemistry, University of Washington, Seattle, WA, USA. [6]Institute for Protein Design, University of Washington, Seattle, WA, USA. [7]Howard Hughes Medical Institute, University of Washington, Seattle, WA, USA. [8]Advanced Engineering Biology Future Science Platform, CSIRO Dutton Park, Brisbane, Queensland, Australia. [9]Research School of Chemistry, Australian National University, Canberra, Australian Capital Territory, Australia. [10]Living Systems Institute, University of Exeter, Exeter, UK. [11]ARC Centre of Excellence for Innovations in Peptide & Protein Science, Brisbane, Australia. [12]Environment Research Unit, Advanced Engineering Biology Future Science Platform, CSIRO Black Mountain Laboratories, Canberra, Australian Capital Territory, Australia. [13]Monod Bio, Seattle, WA, USA. [14]Department of Biosciences, University of Exeter, Exeter, UK. [15]Present address: Department of Biological Sciences, Korea Advanced Institute of Science and Technology, Daejeon, South Korea. e-mail: kirill.alexandrov@qut.edu.au

A commonly cited obstacle in protein switch construction is the paucity of natural domains that undergo a global conformation change upon ligand binding, which is presumed to be required for output control[9]. However, it has long been argued that allosteric regulation is possible in the absence of conformational change[10]. The thermal motion of protein atoms drives the fluctuation among conformations that make up their native state and the changes in fast internal dynamics (conformational entropy) can regulate interaction with other molecules and catalytic efficiency[11]. As almost all artificial protein switches have been constructed using receptor domains with the global conformation, the potential of conformational entropy as an allosteric mediator remains unclear[12]. In this study, we show that ligand-binding domains of diverse ligand classes devoid of global conformation changes, designed by generative machine learning (ML) models, can be converted into efficient biosensor receptors.

## Results

### Construction of β-lactamase chimeras with natural ligand-binding domains

At the start of this study, we searched Protein Data Bank (PDB) for complexes of single-domain proteins with small-molecule ligands that do not undergo global conformation changes upon ligand binding. We selected the anticalin–colchicine complex, where ligand binding results in loop 2 rearrangement and a smaller movement of loops 3 and 4 away from the ligand-binding site[13,14]. We constructed a range of chimeras between TEM-1 β-lactamase and circular permutated anticalin variants (Supplementary Tables 1 and 2). Activity analysis of the resulting recombinant chimeras identified a variant that displayed a dose-dependent response to colchicine with a dissociation constant ($K_d$) value of 33 µM (Fig. 1c). In this chimera the polypeptide segments linking the receptor to the reporter are located opposite the ligand-binding cavity and away from the conformationally flexible loops surrounding it (Fig. 1b). This suggests that circularly permuted ligand-binding domains can function as artificial receptors in chimeric protein switches independently of ligand-induced global conformational changes.

### Protein switches with artificial ligand-binding domains

One limitation of using naturally evolved proteins is the potential presence of alternative conformations not captured by structural analysis that may underlie the observed activity changes. To address this, we tested whether fully artificial ligand-binding domains, which are strongly biased toward biophysically stable single-state proteins, can function as protein switch receptors[15,16]. With this in mind, we tested two small NTF2-family steroid-binding domains designed using ML algorithms[17]. The HCY129.1 domain was reported to display 65 nM affinity for cortisol, while the OHPFA1952 domain has a reported $K_d$ value of 17 nM for 17α-hydroxyprogesterone (17-OHP)[17] (Supplementary Figs. 1a and 2a). These domains were used to generate focused libraries of circularly permuted variants, which were inserted into TEM-1 β-lactamase at position 253 (Fig. 1d). Analysis of the resulting focused libraries identified four cortisol-responsive and three 17-OHP-responsive constructs (Supplementary Tables 1 and 2). The best-performing cortisol chimera displayed a dynamic range of nearly 400-fold and a $K_d$ value of 0.9 µM (Fig. 1e and Supplementary Figs. 1a–d).

The most sensitive 17-OHP biosensor displayed a smaller dynamic range but a much higher affinity for its ligand (Supplementary Fig. 2b–e,i–k). Latency (time required to reach maximal catalytic activity after exposure to saturating concentrations of ligand) of the cortisol biosensor was twice as long as that of the 17-OHP biosensor, which is in line with the notion of thermodynamic coupling of dynamic ranges and response times[8] (Supplementary Figs. 1e and 2g,m). Chimeric proteins, where the binding domains were inserted in their native topology, did not display ligand-dependent activation, suggesting that circular permutation was essential for the emergence of synthetic allostery (Supplementary Figs. 1f and 2h). Analysis of the biosensor's steroid selectivity demonstrated it to be similar to that of the parental ligand-binding domains but could be improved by binding-site randomization and mRNA-based selection (Supplementary Figs. 2c,e and 3 and Supplementary Text 1).

We tested whether ML-designed binders of other ligand types could act as receptors in chimeric protein biosensors. We chose a set of ML-designed minibinders of peptides that have been exhaustively characterized both biophysically and structurally[18–20]. Applying the same workflow, we were able to generate biosensors of BCL-11 and C-peptides that displayed low-micromolar affinity for their targets (Fig. 1f and Supplementary Fig. 4a–d).

We also generated focused libraries of β-lactamase chimeras with circular permutated minibinders of the VirB8-like and MDM2 proteins[15] (Fig. 2g and Supplementary Fig. 4e,f). In both cases, we were able to obtain chimeras with ligand-controlled enzymatic activity (Fig. 1g and Supplementary Fig. 4g). These results suggest that synthetic allostery can emerge in artificial binders of most ligands.

### Diversifying biosensor architecture

Our findings indicate that artificial receptors can be generated from a range of structurally unrelated ligand-binding domains that undergo no obvious global conformation transitions. The developed switches ranged widely in their properties such as latency, affinity, catalytic activity and dynamic range (Supplementary Tables 1 and 2). These properties most likely cannot be optimized simultaneously because of thermodynamical coupling[8]. However, we previously demonstrated that receptor duplication can result in formation of an intramolecular YES-gate that increases its dynamic range while having a modest adverse effect on the latency and the catalytic constant ($k_{cat}$) of the system[21]. As these experiments were performed using natural receptors, we wanted to test whether synthetic receptors are suitable for the construction of intramolecular YES gates[22] (Fig. 2a). To this end, we inserted the circularly permutated 17-OHP binder cpOHPFA1952-31 at positions 41 and 197 of β-lactamase that resulted in >20-fold dynamic range increase (Fig. 2b,c).

Next, we tested whether the artificial receptor domains with orthogonal specificities could be used to construct intramolecular AND gates. We constructed a β-lactamase chimera, where the 17-OHP receptor cpOHPFA1952-31 was introduced at position 41 and the C-peptide receptor cpCPH02-52 at position 197. The resulting chimeric protein displayed a minimal increase in activity in the presence of the individual ligands but its activity increased fivefold in the presence of both ligands (Fig. 2d and Supplementary Fig. 5f).

### Protein switches with alternative reporter domains

During this study, we repeatedly used the β-lactamase reporter domain, prompting a question of whether the synthetic receptors are reporter specific and whether the approach is generalizable. To test this, we constructed chimeras between a circular permutated 17-OHP binder and two alternative reporter enzymes such as PQQ-glucose dehydrogenase (PQQ-GDH) and NanoLuciferase[23,24]. In both cases, we were able to identify steroid-responsive chimeras (Fig. 2e,f and Supplementary Fig. 5e,g–i). These experiments confirm that the developed artificial receptors are autonomous and can be combined with different reporter domains.

### Fully synthetic protein switches

Our results show that allostery can spontaneously emerge in fully artificial ligand-binding domains and regulate natural enzymes. To test whether this extends to artificial reporters, we used the artificial intelligence (AI)-designed luciferase LuxSit Pro[25,26]. We first assessed whether LuxSit Pro can act as an allosteric reporter when combined with natural receptors. To this end, we generated a series of chimeras between LuxSit Pro and calmodulin, a well-established receptor for $Ca^{2+}$ and calmodulin-binding peptides (CaM-BPs)[27,28]. The recombinant chimeras were analyzed for CaM-BP-dependent activity and

https://doi.org/10.1038/s41587-026-03081-9

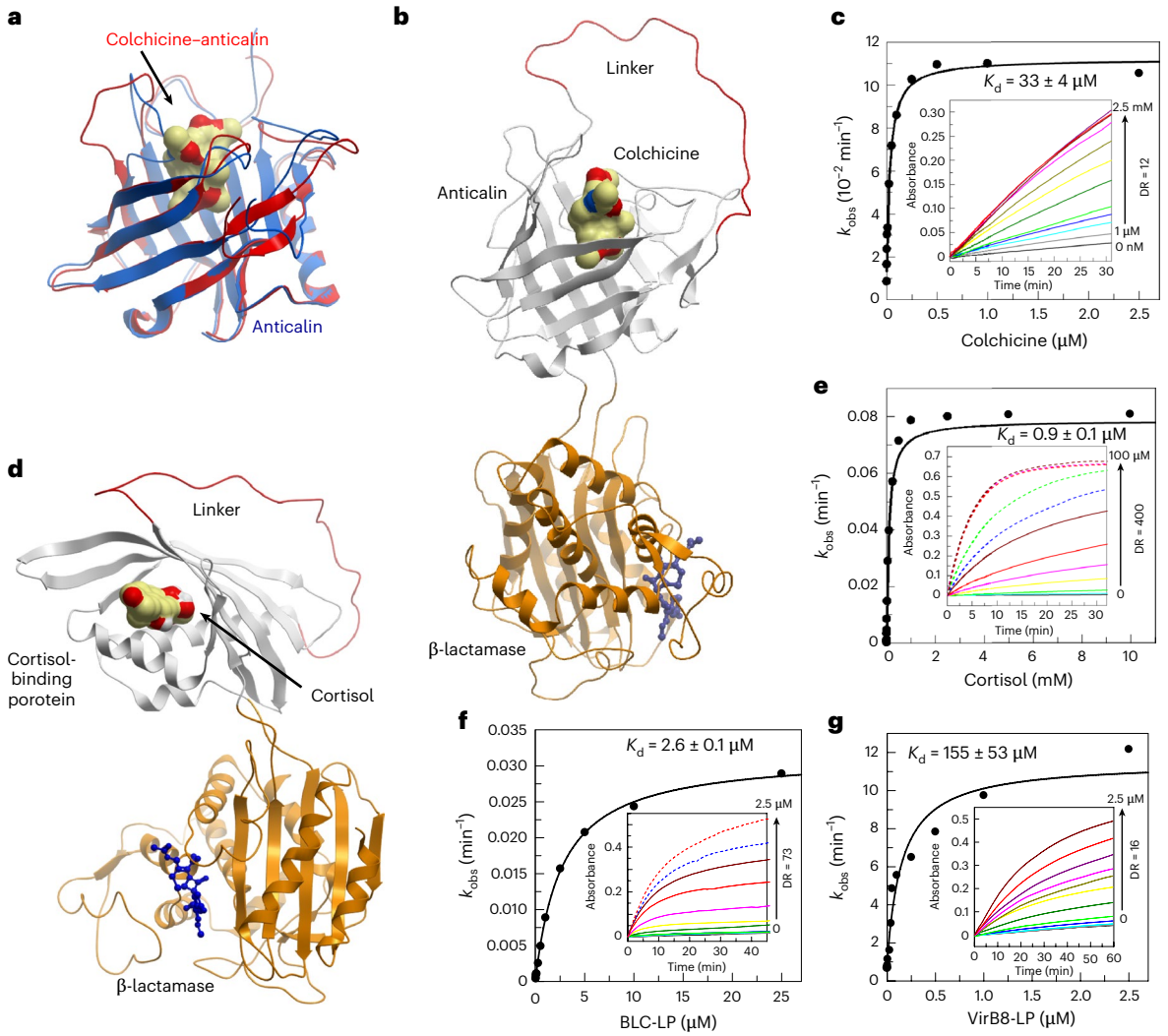


**Fig. 1 | Construction of protein switches with receptor domains devoid of global conformation changes. a**, Superimposition of the anticalin structure in the apo (PDB 5NKN; blue) and colchicine-bound (PDB 6Z6Z; red) states. Colchicine is displayed as molecular surface rendered in atomic colors. The root-mean-square deviation of the superimposed structures is 1.3 Å (0.9 Å without binding-site loops). **b**, Structural model of cpAnticalin-116-BLA-253 chimera with anticalin colored in gray and TEM-1 β-lactamase in gold. The linker connecting the native N and C termini of anticalin is colored red. The active site of β-lactamase is marked by the blue inhibitor molecule imported from PDB 6C79. **c**, Activity analysis of 50 μM chromogenic β-lactamase substrate UW154 following its hydrolysis by 100 nM cpAnticalin-116-BLA-253 chimera in the presence of increasing concentrations of colchicine (inset). The $K_d$ value was calculated by plotting the initial reaction velocities against the ligand concentration and fitting them to a quadratic equation, leading to an apparent $K_d$ value of 33 μM. The dynamic range (DR) is indicated. The methods for estimating s.d. in this and subsequent figures are described in the Methods. **d**, Structural model of a chimera between the NTF2 cortisol-binding domain HCY129.1 and β-lactamase displayed as in **b**. **e**, Enzymatic activity of 50 nM solutions of cpHCY129.1-35-BLA-253 chimera at different concentrations of cortisol. Inset, time-resolved absorbance changes of reactions at increasing concentrations of cortisol. The experiment was performed as in **c**. Fit of the data resulted in a $K_d$ value of 900 nM. **f**, Activity of a 100 nM solution of chimera between the ML-designed BCL-11 peptide-binding protein (PDB 8GJG) and β-lactamase (cpBCL-91-BLA-253) at different concentrations of the ligand peptide. The data were analyzed as in **c**. **g**, Activity analysis of 100 nM cpVirB8-LP-46-BLA-253 chimera in the presence of increasing concentrations of VirB8-LP protein. The data were analyzed as in **c**.

several ON switches with dynamic ranges of 2–4-fold were identified (Supplementary Fig. 6a–c). We then combined CaM insertions at positions 32, 61 and 88 in LuxSit Pro to generate a dual-receptor chimera with a 171–182-fold dynamic range (Supplementary Fig. 6d–f). These observations revealed that efficient allostery is present in both synthetic receptors and synthetic reporters, suggesting that fully synthetic switches may be possible. Activity analysis of chimeras between LuxSit Pro and a circular permutated 17-OHP binder revealed three chimeras with 17-OHP-dependent activity (Fig. 2g and Supplementary Figs. 6g–i). While the catalytic activity of the chimeras was high, they displayed modest (2–3-fold) dynamic ranges. Therefore, we tested whether construction of intermolecular YES gates would improve performance of the system. LuxSit Pro chimeras with two 17-OHP receptors displayed a fivefold increase in dynamic range, confirming that both natural and synthetic chimeras respond in similar ways to receptor duplication (Fig. 2h and Supplementary Figs. 6k–n).

## Functional mechanism of the developed biosensors

Our results demonstrate that it is possible to construct efficient protein switches using ligand-binding domains that do not undergo global conformation transitions. One possible explanation is that such chimeras are misfolded and the presence of the ligand induces a refolding process that ultimately leads to restoration of the reporter's activity. Therefore, we tested whether the introduction of chaotropic agents into the biosensor assay would lower the thermodynamic barrier between OFF and ON states and increase the rate of cpHCY129.135-BLA-253 chimera activation by 17-OHP. Addition of urea to the reaction mixture had no effect on the rate of activation but suppressed the catalytic activity

https://doi.org/10.1038/s41587-026-03081-9

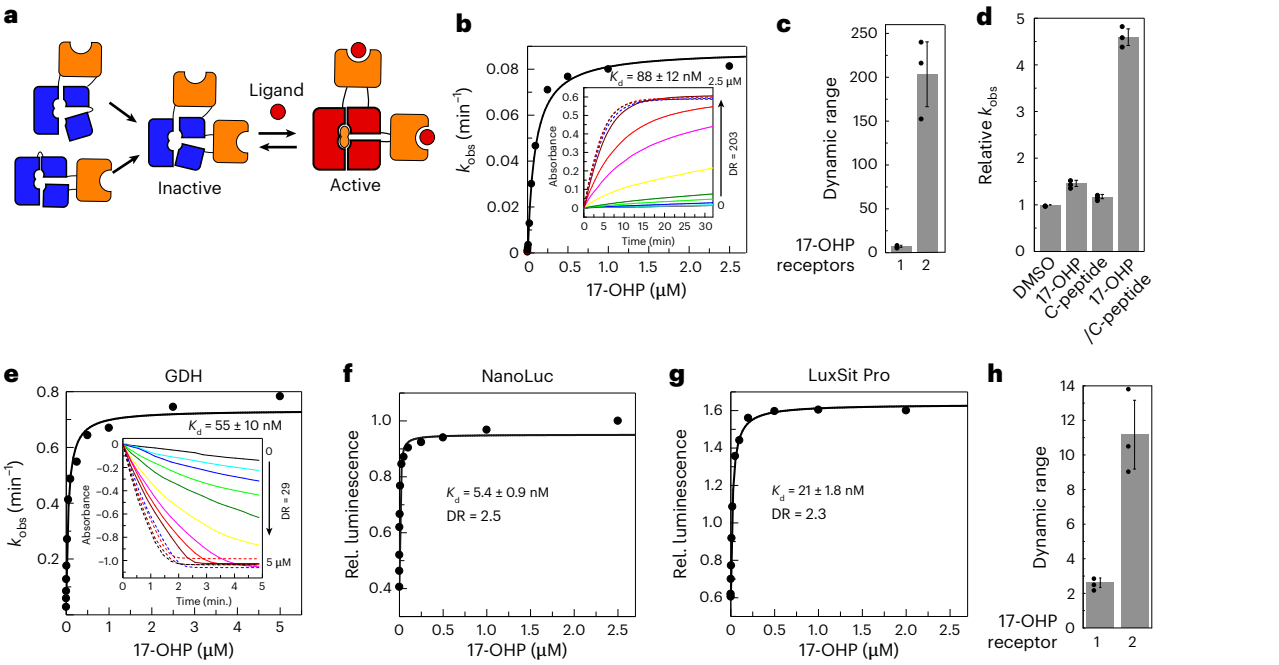


**Fig. 2 | Diversification of biosensor architecture and reporter chemistry.** **a**, Schematic representation of the intermolecular YES-gate protein switch, showing how chimeras with a single receptor domain are compiled into a single chimera containing two receptors. **b**, Activity analysis of a 100 nM YES-gate 2cpOHPFA1952-20-BLA-41-197 chimera titrated with increasing concentrations of 17-OHP. Inset, time traces of the titration reaction used to calculate the $k_{obs}$ values shown in the main plot. **c**, Switch dynamic ranges for constructs containing either one or two 17-OHP receptors (1: cpOHPFA1952-20-BLA-197; 2: 2cpOHPFA1952-20-BLA-41-197). Error bars were calculated using values obtained from three independent reactions. Data are presented as the mean values ± s.d. **d**, Catalytic activity of 100 nM cpOHPFA1952-20-cp-CPH02-52-BLA-41-197 chimera in the presence or absence of 2 µM 17-OHP and 10 µM C-peptide. Error bars were calculated as in **c**. **e**, Activity analysis of a 10 nM solution of cpOHPFA1952-20-GDH-404 in the presence of increasing 17-OHP concentrations. Inset, time traces used for the calculation of $k_{obs}$ values depicted in the main plot. **f**, Relative luminescence values obtained by titrating a 20 nM solution of cpOHPFA1952-20-NanoLuc-157 with increasing concentrations of 17-OHP. The $K_d$ value and dynamic range were calculated by fitting the data to a quadratic equation. **g**, Relative luminescence values obtained by titrating 10 nM chimera of the artificial luciferase LuxSit Pro and a cpOHPFA1952-20 receptor in the presence of LuxSit Pro substrate and increasing concentrations of 17-OHP. **h**, Dynamic ranges of 17-OHP-LuxSit Pro biosensors constructed with one or two 17-OHP receptors (1: cpOHPFA1952-20-LuxSit Pro-61; 2: cpOHPFA1952-20-LuxSit Pro-32-61). The experiment recorded luminescence of 25 nM solutions of each chimera in the presence or absence of 2 µM 17-OHP and these data were used to calculate the chimera's dynamic range. Error bars were calculated as in **c**.

in a dose-dependent fashion (Supplementary Fig. 7a). These results suggest that ligand-induced activity changes of the chimera are not linked to protein folding.

To examine the extent of ligand-induced structural changes in the developed chimeras, we recorded the circular dichroism (CD) spectra of 17-OHP and cortisol binders in their native and circular permutated topology with and without ligand. Figure 3a,b shows that ligands had little effect on the secondary structure of the native and circular permutated 17-OHP binder. In the case of cortisol, we observed slight changes in the spectrum but they were more pronounced in the native protein than in the circularly permutated variant. We repeated these experiments using the native or circular permutated version of 17-OHP and cortisol-binding domain inserted into β-lactamase (Supplementary Fig. 7b–d). Again, the spectra did not reveal notable structure changes.

To gain more insight into changes of chimera structure and dynamics in response to ligand binding, we turned to $^{19}$F-nuclear magnetic resonance ($^{19}$F-NMR) spectroscopy. We used in vivo codon reassignment to install *p*-(O)$CF_3$-tyrosine at positions 105, 229, 230, 256, 389 and 437 of the cpOHPFA1952-20-BLA-253 chimera[29] (Fig. 3d). The sites 256 and 389 are located at the beginning and end of the receptor domain and next to the linker sequences connecting it to the β-lactamase. Positions 229 and 230 are located on the loop connecting β-strand 4 with α-helix 7 of β-lactamase and are adjacent to the N-terminal linker connecting it to the receptor. Residue 105 is located next to the β-lactamase active site while position 437 corresponds to the last C-terminal residue of β-lactamase located far from both the linkers and the active site.

The $^{19}$F-NMR spectra demonstrated that, at every position probed, the addition of saturating concentrations of 17-OHP to the sample resulted in changes in peak height and line shape. The largest change in line width was observed at position 389, which is located at the junction between the last α-helix of the receptor and the linker (Fig. 3d,e). At this site, the binding of the ligand to the binding pocket of the receptor results in either a more homogeneous environment of the fluorine probe or faster averaging between different conformations. In either case, the nonsymmetric line shape of the signal indicates that some conformational heterogeneity persists. Heterogeneity is not unexpected as the last α-helix of the receptor forms the bottom of the ligand-binding pocket and the circular permutation is expected to increase its entropy compared to the wild type because of the introduction of a long unstructured loop preceding it (Fig. 3d,e). The spectra collected with the protein containing the label at position 256 also showed a change in peak position and line shape. These changes were less pronounced than at position 389 but the line shape in the presence of ligand was still nonsymmetric. The probes at positions 229 and 230 reported nearly identical ligand-induced changes, resolving two main components of similar intensity. The probe installed at position 105 is located at the edge of the β-lactamase active site. It is located far from the ligand-binding domain, yet reports a small but notable change in signal intensity and the appearance of a small shoulder in the ligand-bound state, demonstrating the reach of the allosteric effect (Fig. 3f). The probe at position 437 was chosen as a reference peripheral to the allosteric path of signal transmission. Nonetheless it also displayed distinct

https://doi.org/10.1038/s41587-026-03081-9

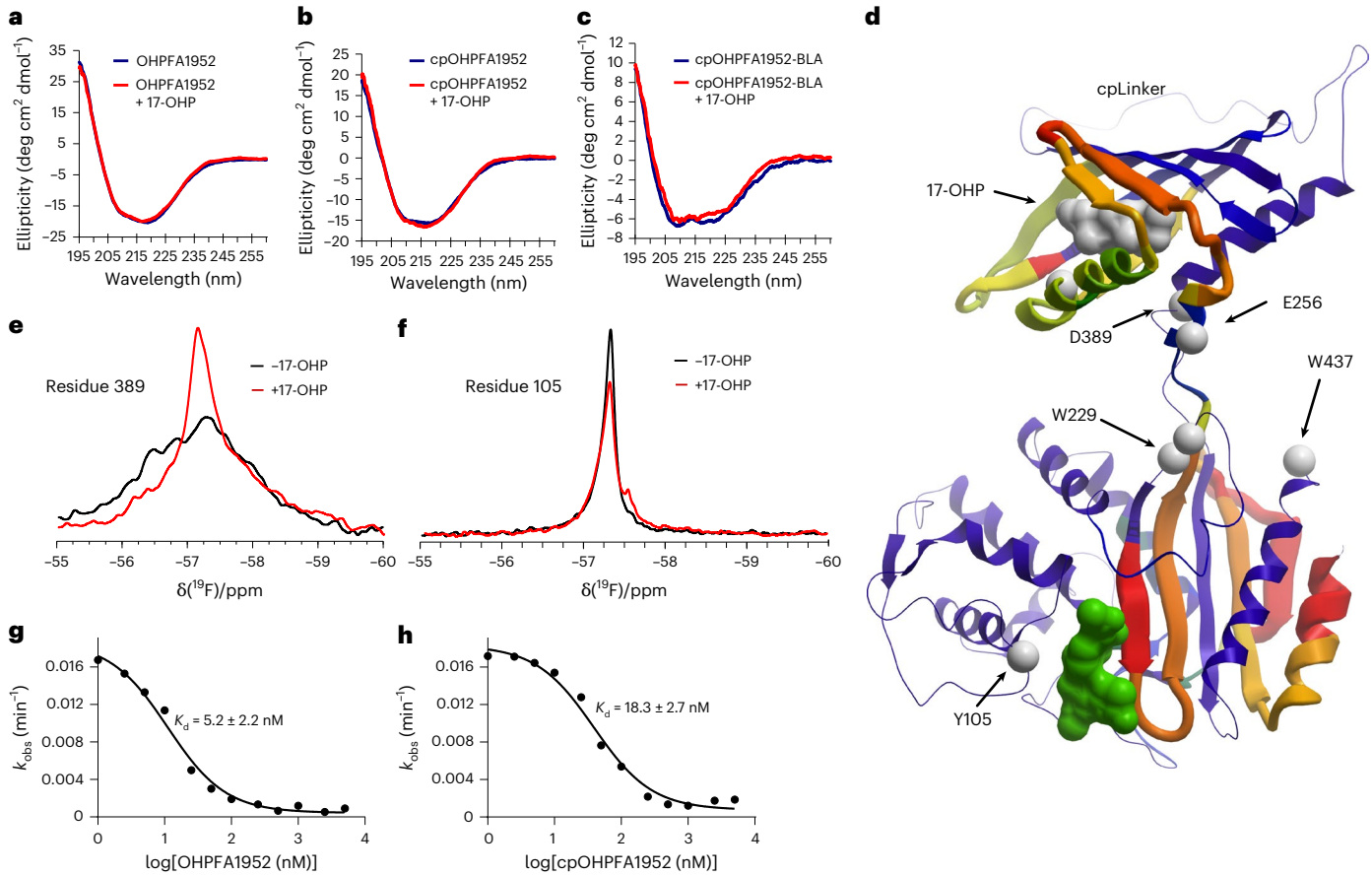


**Fig. 3 | Functional mechanism of the developed allosteric chimeras. a**, Far-UV CD spectra of 6.7 µM 17-OHP-binding domain OHPFA1952 in the absence (blue line) and presence (red line) of 20 µM 17-OHP. **b**, As in **a** but using 6.4 µM circularly permutated OHPFA1952. **c**, As in **a** but using 2.2 µM cpOHPFA1952-20-BLA-253 chimera. **d**, Structural model of cpOHFPA_1952-20-BLA-253 bound to 17-OHP (gray molecular surface) colored according to the relative stability difference between apo and holo forms from HDX analysis. Large changes in exchange rates are also represented by thicker ribbons. The Cα atoms of the amino acids that were replaced with *p*-(O)$CF_3$-tyrosine are displayed as gray balls and labeled. The active site of β-lactamase is marked by the active-site inhibitor imported from PDB 6C79 displayed as molecular surface colored in green. **e**, $^{19}$F-NMR spectra of 0.6 mM cpOHPFA1952-20-BLA-253 labeled with *p*-(O)$CF_3$-tyrosine at position 389 in the absence (black line) and presence of 1.5 mM 17-OHP. **f**, As in **e** but using cpOHPFA1952-20-BLA-253 labeled at position 105. **g**, Activity analysis of reactions containing 100 nM cpOHPFA1952-20-BLA-253, 50 nM 17-OHP, 50 µM UW154 and indicated concentrations of OHPFA1952. The titration data were fitted to a competitive equation to determine the $K_d$ value of 17-OHP:OHPFA1952 interaction. **h**, As in **g** but titrating with cpOHPFA1952-20.

spectral changes. All protein mutants containing *p*-(O)$CF_3$-tyrosine displayed catalytic activity and switchability, suggesting that the changes sensed by the fluorine probes reflect conformational variability intrinsic to the biosensor (Supplementary Fig. 8e).

To put the observed changes in the environment of individual residues into a global context, we performed hydrogen/deuterium exchange mass spectrometry (HDX–MS) and molecular dynamics (MD) simulations of cpOHPFA1952-20-BLA-253 and wild-type OHPFA1952-20-BLA-253 in the presence and absence of saturating concentrations of 17-OHP. While results of the MD simulations were inconclusive (Supplementary Figs. 9 and 10 and Supplementary Text 2), the HDX–MS experiments generated interpretable data. Amide HDX rates directly relate to local structural dynamics and can be routinely determined in large protein systems, with millisecond-time and single-amino-acid resolution[30]. Equilibrium exchange experiments with EX2 kinetics as observed here reflect local stability throughout the protein chimera[31]. The pattern of stability changes in both proteins upon 17-OHP binding showed some similarity but the magnitude of changes was approximately tenfold larger in the circularly permuted chimera than with the wild-type receptor. This large difference encompasses 17-OHP-induced stabilization of the cpOHPFA domain and stabilization of the β-lactamase core including its active site (Fig. 3d and Supplementary Fig. 11a–d).

The analysis of NMR and HDX–MS data points to a potentially important role of the linker sequences connecting the receptor and reporter domains. We tested the sensitivity of our system to the linker structure by introducing additional glycine residues into the linker connecting the last α-helix of the receptor and β-strand 8 of β-lactamase. Increase of the linker length by introducing glycine residues stepwise reduced the dynamic range but increased the maximal catalytic rate. Rigidification of the longer linkers through introduction of serine residues reverted the effect (Supplementary Fig. 11e).

To understand the effect of circular permutation on ligand-binding domains, we performed competitive titrations, where either the wild-type or circular permutated OHPFA1952-20 binder was titrated into a mixture of 2cpOHPFA1952-20-BLA-41-197 and 17-OHP. The resulting data were fitted to a competitive titration model, yielding an estimate of the $K_d$ values of the binding of 17-OHP to either binder. Circular permutation resulted in a ~4-fold decrease in the receptor affinity for its ligand (Fig. 3g,h). The affinity determined is very close to that of the cpOHPFA1952-20-BLA-253 biosensor for 17-OHP. The difference in affinity was corroborated by isothermal titration calorimetry (ITC) experiments (Supplementary Fig. 12h,k). We repeated these experiments using cortisol binder HCY129.1 and its permutated version cpHCY129.1-35. Within the uncertainty of the fit, the apparent $K_{Dd}$ was fourfold lower for the permutated cortisol binder (Supplementary Fig. 12a,b).

https://doi.org/10.1038/s41587-026-03081-9

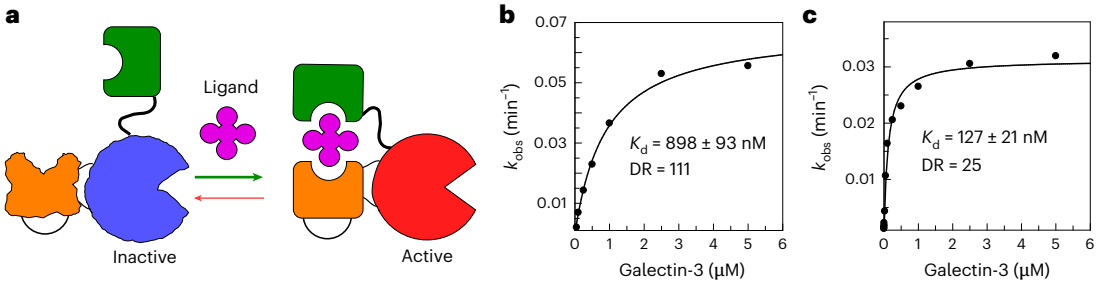


**Fig. 4 | Protein switches with intramolecular dimerization system.** **a**, Schematic of a switch with intramolecular dimerization system that offsets the entropic penalty of circular permutation of the receptor. A second binder present in *cis* increases both the association rate and decreases the dissociation rate, offsetting the entropic penalty created by circular permutation of the receptor domain. **b**, Activity analysis obtained by titrating a 25 nM solution cpFN3conB9-62-BLA-253 with an increasing concentration of Gal-3. **c**, As in **b** but using cpFN3conB9-62-BLA-253-FN3con-B41, which contains an additional Gal-3-binding domain.

To gain insight into the kinetics of the receptor–ligand interaction, we performed biolayer interferometry experiments using 17-OHP-PEG-biotin conjugate immobilized on a streptavidin chip. The association rate constant ($k_{on}$) of the wild-type HCY129.1 domain was approximately twice as fast as that of the cpHCY129.1-35 while the dissociation rate was approximately 2.5 times slower (Supplementary Fig. 12f,g). These rates are consistent with fivefold affinity differences between wild-type and circular permutated receptor. We note that these values are approximate, as the PEG linker and streptavidin affected the 17-OHP–receptor interactions (Supplementary Fig. 12c–e).

These observations support the idea that the increased conformational entropy of the circularly permutated ligand-binding domains negatively impacts the kinetics of the interaction and, therefore, the overall affinity of the ligand–binder complex. We hypothesized that this entropic penalty could be offset by introducing an additional specific ligand-binding domain that would increase the local concentration of the ligand. This would increase its association rate and, through cooperative action with allosteric receptor, reduce the dissociation rate and increase the overall affinity of the system (Fig. 4a). To test this idea, we took advantage of the FN3con binding domains B9 and B41 selected against cardiac failure biomarker Galactin-3 (Gal-3). The $K_d$ value of the FN3Con-B9 interaction with Gal-3 was 2.2 nM while FN3Con-B41 bound to the complex of Gal-3:FN3Con B9 with a $K_d$ of 1 nM (ref. 32). The cpFN3conB9-62-BLA-253 chimera displayed a dynamic range of 111-fold (Fig. 4b). However, the affinity of the system for Gal-3 was markedly reduced to ~0.9 μM, which is in line with the previous observations[33] (Fig. 4b). We then fused the B41 binding domain by a flexible linker to the C terminus of the chimera and tested the response of the resulting protein to Gal-3. This system displayed a sevenfold increase in affinity, confirming that the circular-permutation-mediated affinity reduction can be at least partially offset by auxiliary binding domains.

### Construction of *Escherichia coli* strains controlled by β-lactamase switches with synthetic receptors

Gram-negative bacteria expressing β-lactamase in their periplasm gain resistance to β-lactam antibiotics. This led us to explore whether expression of the developed biosensors in *E. coli* cells would make them 'addicted' to their cognate ligands. To this end, we constructed recombinant *E. coli* strains that expressed cortisol and 17-OHP biosensors in the periplasm under the control of a constitutive promoter. The resulting strain was able to grow on both liquid and solid media supplemented with ampicillin only in the presence of the cognate ligands (Fig. 5a,b and Supplementary Fig. 13a,b).

### Sensory bioelectrodes based on protein switches with artificial receptors

Enzyme-based assays are unmatched in their simplicity, speed and cost-effectiveness, as exemplified by both endpoint and continuous glucose monitoring[34]. It has long been hoped that artificial protein biosensors will deliver diagnostic tests of similar efficiency for a wide range of biomarkers. The biosensors developed in the present work, with their single-component architecture, large dynamic range, high catalytic activity and compatibility with an electrochemical readout, are promising candidates for novel sensing applications. Therefore, we tested whether our PQQ-GDH-based protein switches, which produce electrons as a byproduct of glucose oxidation, can be used to construct electrochemical sensory bioelectrodes. We covalently attached the cpOHPFA1952-20G-GDH-404 chimera to the graphene nanosheets on the surface of carbon electrodes (Supplementary Fig. 13d). The electrodes were analyzed by cyclic voltammetry in the presence or absence of saturating concentrations of glucose and 17-OHP (Fig. 5d,e). At saturating concentrations of glucose, the electrode produced current in proportion to 17-OHP concentration. These data could be fitted to a $K_d$ value of 34 nM, which is close to that determined using the solution-based assay (Fig. 2e). The electrode activity could be reset to baseline by washing off 17-OHP, thereby allowing for multiple cycles of activation and deactivation (Fig. 5e).

## Discussion

Single-component protein biosensors offer several advantages over multicomponent systems[6]. However, their construction is predicated on the availability of receptor domains with suitable specificity, affinity, size and topology for functional coupling to a reporter domain.

We evaluated the suitability of ML-designed ligand-binding domains as biosensor receptors. This approach tends to produce highly stable proteins with reduced conformational dynamics[16]. We combined circularly permutated variants of ML-designed domains with TEM-1 β-lactamase to obtain 47 protein switches activated by different ligand classes. These switches exhibited substantial variation in affinity, dynamic range, response time and catalytic activity. The chimeras consistently showed reduced ligand affinity compared to their parental domains, with decreases ranging from severalfold to orders of magnitude. Response times also varied, from minutes to tens of minutes. This reveals a rugged fitness landscape, indicating substantial scope for optimization across multiple performance parameters. We demonstrated a combination of switches with modest (2–5-fold) dynamic ranges into two receptor YES-gate chimeras with dynamic ranges > 200-fold[21]. This offers a practical alternative to the multiple rounds of mutagenesis and linker optimization traditionally used to enhance single-component biosensor performance[35,36]. The small size of ML-generated ligand-binding domains makes this approach particularly attractive[16]. We assessed the autonomy of the synthetic receptors by transplanting them into alternative reporter domains, including the luminescent NanoLuciferase, redox enzyme PQQ-GDH and, ultimately, ML-designed luminescent protein LuxSit Pro.

Biophysical analyses using CD, $^{19}$F-NMR and HDX–MS showed that ligand binding does not induce refolding or global conformational

https://doi.org/10.1038/s41587-026-03081-9

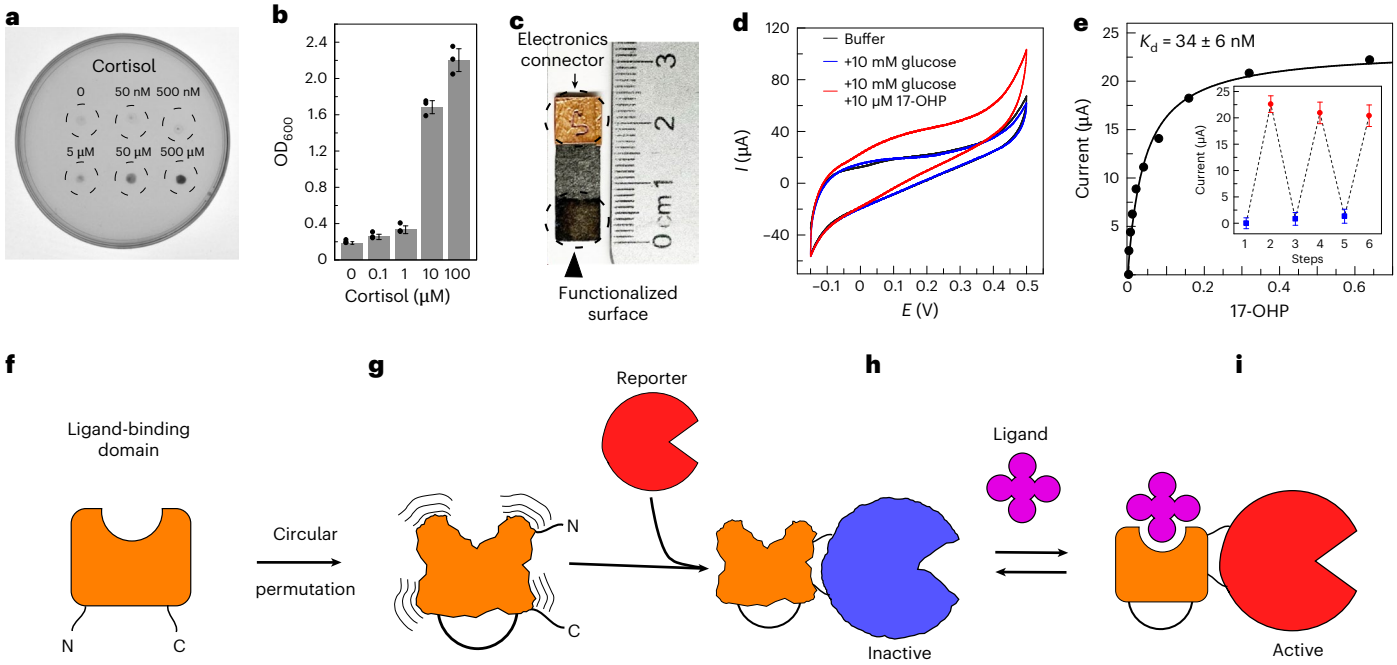


**Fig. 5 | Applications of the developed biosensors. a**, Agar plate containing ampicillin and chloramphenicol antibiotics seeded with *E. coli* strain DH5α expressing cpHCY129-35-BLA-253 chimera. After bacterial plating, 2 µl of cortisol solution at the concentration indicated was spotted in the marked positions and bacterial growth was allowed to proceed overnight. **b**, Density plot of *E. coli* DH5α suspension cultures of cpHCY129-35-BLA-253 in LB liquid medium in the presence of different concentrations of cortisol. Error bars were calculated using values obtained from three independent bacterial cultures derived from different clones of a single transformation. Data are presented as the mean values ± s.d. $OD_{600}$, optical density at 600 nm. **c**, Photograph of carbon/graphene electrode functionalized with 17-OHP-GDH biosensor. The section of the electrode functionalized with the biosensor and the electronic connector are framed and labeled. **d**, Typical cyclic voltammograms for a bioelectrode based on cpOHPFA1952-20G-GDH-404. Black line: 25 mM HEPES pH 7.2, 100 mM $Na_2SO_4$ and 3 mM calcium acetate; blue line: 10 mM glucose added; red line: 10 mM glucose and 5 µM 17-OHP added. The electrode was scanned at a rate of 5 mV $s^{-1}$ versus reference electrode (Ag/AgCl/3 M KCl) at room temperature. **e**, Increase in the electric current on the 17-OHP-GDH bioelectrode shown in **c**,**d** following its exposure to increased concentrations of 17-OHP. Inset, electrode current following repeated addition and removal of 17-OH. Error bars were calculated using values obtained from three independent scans of the same electrode under the corresponding conditions. Data are presented as the mean values ± s.d. **f**–**h**, Proposed functional mechanism of protein switches with artificial circular permutated receptor domains (**f**), where circular permutation increases the conformation entropy of the receptor domain (**g**) that propagates to the reporter domain suppressing its activity (**h**). **i**, Binding of a ligand reduces the conformation entropy of the system and increases the catalytic activity of the reporter domain.

changes in the chimeras. Instead, their behavior is consistent with circular permutation reducing receptor cooperativity, increasing conformational entropy and thereby suppressing reporter catalytic activity (Fig. 5f–i). The reduced ligand affinity of the chimeras relative to the native binders is consistent with increased conformational entropy that is not fully offset by binding enthalpy. Although this represents a potential limitation, we show that auxiliary binding domains can mitigate the entropic penalty.

The small size of ML-generated binding domains markedly reduces circular permutation library complexity (fewer than ten variants in our case), enabling rapid and cost-effective identification of input-responsive switches. However, thermodynamic coupling across performance parameters may necessitate advanced optimization strategies[8]. Both directed evolution and ML approaches have proven effective for tuning allosteric proteins[37,38]. The ability of design switches with input and output parameters of choice will support the development of switch-based circuits with signal amplification, noise suppression and logic capabilities, paving the way for applications in diagnostics, analytics and biorthogonal real-time signal processing in engineered organisms.

# Method

## Materials

Cortisol, 17-OHP, 2,6-dichlorophenolindophenol (DCPIP), phenazine methosulfate (PMS), pyrroloquinoline quinone (PQQ), 1-ethyl-3-(3-dimethylaminopropyl)carbodiimide (EDC), *N*-hydroxysuccinimide (NHS) and polyethyleneimine (PEI) were purchased from Sigma-Aldrich. Compound UW154 was commercially synthesized by o2h Discovery[39]. NanoLuc substrate furimazine was purchased from Promega. Deuterated chemicals were purchased from Goss Scientific Instruments. The LuxSit Pro assay kit was acquired from Monod Bio (LS0101). The luciferase assay plate OptiPlate-96 HS was purchased from PerkinElmer. The synthetic peptides were purchased from Mimotopes. Biotinylated 17-OHP with a PEG linker and biotinylated cortisol with a PEG linker were synthesized by SYNthesis med chem. Biotinylated progesterone with a PEG linker was purchased from Cayman Chemical (9000645).

## Molecular cloning, expression and purification of recombinant proteins

The open reading frames of the constructs listed in Supplementary Table 1 were synthesized commercially (Gene Universal) and cloned into a kanamycin-resistant pET-28a(+) vector.

Competent *E. coli* BL21(DE3) cells (New England Biolabs) were transformed with the resulting expression vectors and grown in Luria–Bertani (LB) broth with 50 µg $ml^{-1}$ kanamycin (Everest) with shaking at 37 °C. Protein expression was induced by adding 0.3 mM IPTG (Sigma) and the cultures were incubated overnight at 18 °C. Cells were harvested at 4,000 rpm for 10 min and the cell pellet was lysed in buffer containing 50 mM $Na_2HPO_4$ (pH 8.0), 300 mM NaCl, 20 mM imidazole, 1 mM AEBSF and DNAse I (all Sigma). Following cell lysis and disruption at 27 kPsi using the CFII cell disrupter (Constant Systems), the supernatant was collected and recombinant protein was further purified on

the Ni-NTA HisTrap FF crude column driven by ÄKTA Express purifier (Cytiva) system in buffer containing 50 mM $Na_2HPO_4$, 300 mM NaCl and 20 mM imidazole and a gradient of 500 mM imidazole for elution at pH 8.0. Finally, the protein was dialyzed against 20 mM Tris-HCl (pH 7.0) and 100 mM NaCl; protein aliquots were frozen in liquid nitrogen and stored at −80 °C.

### Design of chimeric proteins

To design the protein chimeras, a arbitrary residue located within a loop region was chosen as the permutation site to generate the circularly permuted binder. This amino acid was removed to establish novel N and C termini. The native N and C termini of the binder were joined by a flexible glycine–serine linker of sufficient length. This permuted binder was inserted at position 253 of β-lactamase TEM-1, with a single glycine residue used as a linker between TEM-1 and the binder. The structural models of the chimeras were generated using WinCoot 0.9.8.1 and the structures of the receptor and reporter domains as inputs. The structure of TEM-1 β-lactamase (PDB 3GMW) was manually connected to the structure of the circularly permuted binders and the linker joining the native N and C termini of the binder was manually constructed. The structures of proteins and protein chimeras were visualized using ICM 3.9-4 (Molsoft).

### Expression and purification of protein containing NMR probe

For the site-specific incorporation of the unnatural amino acid *p*-(O)$CF_3$-tyrosine, *E. coli* B-95.ΔAΔ*fabR* cells[40] (Addgene, 197934) were cotransformed with pRSF-G1-pCNPRS (Addgene, 174719) and the pCDF plasmids (Gene Universal) carrying the gene of the target with amber codon placed at the desired position. The cells were grown in LB medium (Sigma) supplemented with 25 mg $L^{-1}$ kanamycin (Everest) and 25 mg $L^{-1}$ spectinomycin at 37 °C until reaching an optical density of 0.4–0.6, followed by the addition of *p*-(O)$CF_3$-tyrosine (Ambeed) to the final concentration of 2 mM. After 30 min of continuous shaking, IPTG (Sigma) was added to a final concentration of 0.5 mM to induce protein expression and the culture was grown overnight at 18 °C. The recombinant protein was purified by Ni-NTA chromatography using a HisTrap FF crude column driven by an ÄKTA Pure Purifier (Cytiva) system as described above.

### $^{19}$F-NMR spectroscopy

$^{19}$F-NMR spectra were recorded using protein samples at 0.40–0.85 mM concentration dissolved in 90% $H_2O$/10% $D_2O$, 20 mM Tris-HCl pH 7.2 and 100 mM NaCl and placed in 5-mm NMR tubes. The ligand 17-OHP was added from a 100 mM stock solution in DMSO at a final concentration of 1.5 mM. $^{19}$F-NMR spectra were recorded at 25 °C without $^1$H decoupling on a Bruker 400-MHz NMR spectrometer equipped with a broadband probe. The following parameters were used: acquisition time, 180 ms; recovery delay, 1 s; exponential window multiplication with line broadening by 15–40 Hz (depending on the natural line width) before Fourier transformation. The total recording times of the NMR spectra ranged between 0.5 and 1 h. Inversion–recovery experiments determined $T_1$ relaxation times of about 0.6 s.

### Design of small-molecule-binding proteins

De novo proteins binding cortisol and 17-OHP were designed as previously described[17]. Protein backbone scaffolds were generated using a hallucination method based on trRosetta to generate diverse structures with NTF2-like topology. Cortisol and 17-OHP were docked onto these scaffolds using RIFdock and protein sequences were subsequently designed with either using Rosetta or LigandMPNN[41]. The resulting ligand–protein complexes were evaluated using Rosetta scoring functions and AlphaFold2 predictions. Selected subsets of sequences were experimentally tested for binding characterization and representative binders were then chosen for the construction of chimeric sensor proteins.

### Design and construction of C-peptide binding domain

CPH02 was optimized from the construct CPS_1b2 in the previous work[42]. Here, full length C-peptide was remodeled with the designed binder instead of a short middle region. The ProteinMPNN-fastrelax[43] cycle was carried out twice to refine the interface toward the new dock, with arginine and lysine downweighted by −0.15. Ten new sequences were generated and the top design with the best AlphaFold2 metrics[42] was selected, characterized biophysically and used for biosensor design.

### ELISA assay

To achieve streptavidin (Sigma, S4762) immobilization on a Maxisorp plate (Thermo Fisher Scientific, 442404), the latter was incubated with 10 μg $ml^{-1}$ streptavidin in PBS solution overnight at room temperature. The plate was washed three times with PBS, incubated with 2 μM biotinylated steroids for 1 h and then blocked with 2% casein in PBS for 1 h. Purified binding proteins were serially diluted in 2% casein in PBS buffer. After a 1-h incubation, the plate was washed three times with PBST (PBS with Tween-20) and incubated for 1 h with 100 μl of anti-FLAG–HRP (1:5,000; Sigma, A8592). Following PBST washes, TMB substrate (Thermo Fisher, 34028) was added and the reaction was quenched with 1 M sulfuric acid when the color developed sufficiently. Absorbance at 450 nm was recorded using a Neo2 plate reader. The titration data were fitted in GraphPad Prism using its four-parameter $IC_{50}$ equation and the resulting values were used as the apparent affinity estimate.

### Spectrophotometric analysis of β-lactamase enzymatic activity

The enzymatic assays were performed in the assay buffer containing 20 mM Tris-HCl pH 7.2 and 100 mM NaCl at 25 °C by monitoring the increase in absorbance of UW154 (ref. 39) at 520 nm using a Cary 60 ultraviolet (UV)–visible light (Vis) absorbance spectrometer operated by Cary WinUV Software.

### Spectrophotometric analysis of GDH enzymatic activity

The GDH chimera protein was reconstituted with PQQ in 1:1.5 ratio. The enzymatic assays were performed in the assay buffer containing 20 mM Tris-HCl pH 7.2, 1 mM $CaCl_2$ and 100 mM NaCl in the presence of 60 μM electron-accepting dye DCPIP, 0.6 mM electron mediator MPS and 20 mM glucose at 25 °C by monitoring the decrease in absorbance at 600 nm using a Cary 60 UV–Vis absorbance spectrometer operated by Cary WinUV Software.

### Analysis of NanoLuc enzymatic activity

The assay was performed in 96-well plates (OptiPlate-96 HS, PerkinElmer). The luminescence was recorded at 445–470 nm by a TECAN plater reader after mixing 200 μl of a solution containing 20 mM Tris-HCl pH 7.2, 100 mM NaCl and 0.25 μl of the NanoLuc substrate and NanoLuc chimera protein.

### Analysis of NanoLuc and LuxSit Pro enzymatic activity

The enzymatic assay of NanoLuc and LuxSit were performed in 200 μl of buffer containing 20 mM Tris-HCl pH 7.2 and 100 mM NaCl or the supplied assay buffer from LuxSit Pro luciferase assay system, respectively. The protein sensors were first incubated at 25 °C for 30 min with corresponding ligands. Upon addition of 0.2 μl of substrate (NanoLuc, Promega) or 2 μl of substrate (LuxSit Pro substrate, Monod Bio), the change in luminescence signal at 445–470 or 475–500 nm, respectively, was monitored with a TECAN plater reader (SPARK).

### Activity analysis of β-lactamase calmodulin chimera library in the presence of different CaM-BPs

A set of 17 genes encoding β-lactamase–CaM chimeras were synthesized and named on the basis of the residue in β-lactamase where the CaM domain was inserted (Supplementary Table 1). The chimeras were

recombinantly produced in *E. coli* and their activity was tested in the presence of 29 CaM-BPs to evaluate the effects of both insertion site and ligand peptide on biosensor function using a 96-well plate assay format. The purified β-lactamase–CaM proteins were prepared at a final concentration of 10 nM in a reaction buffer containing 20 mM Tris-HCl pH 7.2 and 100 mM NaCl. Enzymatic activity was assessed for each variant in both the presence and the absence of 1 μM CaM-BPs. Following peptide addition, the biosensor–peptide mixtures were incubated at room temperature for 20 min. To ensure simultaneous reaction initiation, 50 μM nitrocefin was added to each well of the 96-well plate using the Rainin Liquidator 96 manual pipetting system. Absorbance of the solution at 486 nm was continuously recorded every 10–20 s at 25 °C using a Synergy Neo2 microplate reader (BioTek) until the signal stabilized.

### Quantification of biosensor performance parameters and data plotting

To determine the dynamic range of the individual switches, we used ligand titration experiments to establish the $K_d$ value for the ligand. We then performed the assay either at zero or saturating concentration of the ligand (typically 20-fold greater than the $K_d$ value) and recorded the absorbance change trace. The linear phase of the trace was fitted to the linear function defined as the observed rate constant ($k_{obs}$). The dynamic range was calculated by dividing the $k_{obs}$ of the background signal in the absence of the ligand by the $k_{obs}$ recorded at saturating ligand concentration.

To determine the biosensor's latency, the switches were incubated with their cognate ligands for the time period indicated and assayed for enzymatic activity. The initial rates were determined and the activation rate was calculated by fitting the data to a single exponential.

To determine the affinity of the biosensors for their targets, the linear phase of the curves recorded at different concentrations of the ligand was fitted as a linear function to obtain $k_{obs}$. The mean $k_{obs}$ was obtained by averaging three independent experimental data. To obtain the $K_d$ for the interaction of biosensors with their ligand, the $k_{obs}$ data were plotted against the concentration of the ligand and the data were fitted to the explicit solution of equation 1 describing the E + S < > ES binding equilibrium, where $K_d$ is defined as $K_d = [E] \times [S]/[EL]$. $[E_0]$ and $[L_0]$ refer to the total enzyme and ligand concentration (free and bound) in the cuvette. Under these conditions, $k_{obs}$ can be expressed as follows:

$$k_{obs} = k_{obs(min)} + (k_{obs(max)} - k_{obs(min)}) \times (([E_0] + [L_0] + K_d)/2 - ([E_0] + [L_0] + K_d)^2/4 - [E_0] \times [L_0])^{1/2}/[L_0] \quad (1)$$

where $k_{obs}$ represents the measured rate, and $k_{obs(min)}$ and $k_{obs(max)}$ refer to the minimal and maximal rates observed, respectively. A least-squares fit of the data to equation 1 using the software package Grafit 5.04 (Erithacus software) was used to extract the $K_d$ value and its s.d.

In competitive titrations aimed at determination of the $K_d$ values for 17-OHP interaction with OHPFA1952 or cpOHPFA1952-20, the mean $k_{obs}$ values from three independent experiments were fitted to a competitive model using GraphPad Prism 10.4.1. In this process, we used the one-site fit inhibition constant ($K_i$) model and fixed the $K_d$ of cpOHPFA1952-20-BLA-253 interaction with 17-OHP to the value obtained in direct titration of cpOHPFA1952-20-BLA-253 with 17-OHP.

The bars in the bar graphs shown in Figs. 3 and 4 represent values of an average of three independent measurements performed as a part of the same experimental set. The error bars denote positive and negative boundaries of the s.e.m.

### Construction of expression vectors for in vivo activity analysis of β-lactamase and bacterial survival assays

The constructs carrying β-lactamase chimeras with a constitutive promotor based on a modified pACYCDuet-1 vector were created. The inducible T7 promotor in the original pACYCDuet-1 vector was replaced by the constitutive AmpR promotor (Supplementary Table 1).

### Thermostability analysis of the β-lactamase-based biosensor

We incubated the β-lactamase-based switches in triplicates at different temperatures before the activity assay. The incubation times and temperatures were as follows: 4 °C for 3 h, 25 °C for 3 h, 37 °C for 1 h, 50 °C for 30 min, 50 °C for 10 min and 80 °C for 10 min.

### CD spectrum recording

CD spectra were measured using a J-1500 Spectropolarimeter (Jasco) within the wavelength range of 194–260 nm. Data were collected at 0.1-nm intervals with a path length of 1 mm and a scanning speed of 50 nm $min^{-1}$. The experiments were conducted in triplicate using protein samples prepared in a buffer containing 10 mM Tris-$H_2SO_4$ pH 7.2 and 20 mM NaCl with or without the ligand. The concentrations of both the protein and the ligand used in the assays are detailed in the respective figure legends.

### Biolayer interferometry

Binding kinetics were measured on an Octet RED968 system (ForteBio) at 25 °C using streptavidin biosensors. Sensors were preequilibrated in assay buffer (PBS, 0.05% Tween-80 and 0.1% BSA) before ligand loading. A biotinylated 17-OHP derivative (200 nM) was immobilized to a loading response of ~0.35 nm, followed by baseline stabilization in assay buffer.

Association was measured by dipping sensors into wells containing wild-type OHPFA1952 17-OHP-binding domain or the circularly permuted variant cpOHPFA1952-20 at 400, 200, 100 and 0 nM. After 300 s of association, sensors were transferred into buffer-only wells to monitor dissociation for 300 s. Reference sensors (ligand-loaded, buffer only) were included to subtract background.

Data were reference-subtracted, aligned and globally fitted to a 1:1 binding model using ForteBio Data Analysis 9.0 to obtain association ($k_{on}$) and dissociation ($k_{off}$) rate constants, as well as the equilibrium dissociation constant ($K_d$).

### ITC

ITC experiments were performed on a MicroCal PEAQ-ITC (Malvern) at 25 °C. Proteins were dialyzed extensively against assay buffer (20 mM Tris-HCl pH 7.2 and 100 mM NaCl). Protein concentrations were determined spectrophotometrically using calculated extinction coefficients. 17-OHP was dissolved in DMSO (20 mM) and diluted to 50 μM in the same buffer.

The sample cell (200 μl) was loaded with 50 μM 17-OHP and the syringe (40 μl) contained 500 μM wild-type OHPFA1952 or cpOHPFA1952-20. Each titration consisted of an initial 0.4-μl injection followed by 19 sequential 2-μl injections, with a reference power of 10 μcal $s^{-1}$ and stirring at 750 rpm. Control titrations of protein into buffer were performed to correct for dilution heats.

Raw thermograms were integrated, corrected for heats of dilution and fitted to a one-site binding model using the MicroCal PEAQ-ITC analysis software. Thermodynamic parameters including $K_d$, enthalpy ($\Delta H$), entropy contribution ($-T\Delta S$) and Gibbs free energy ($\Delta G$) were derived from the fits.

### Preparation of bioelectrodes functionalized with 17-OHP-GDH biosensor

Carbon paper composed of carbon fibers (SpectracarbTM 2050 L-1050, Fuel Cell Store) was used as the core electrode material. To increase the sensitivity of the bioelectrode, the carbon fibers were decorated with graphene nanosheets using four cycles of cyclic voltammetry in the range of −0.5 to +3.0 V, with a potential scan rate of 50 mV $s^{-1}$ for four successive cycles in 25 mM phosphate buffer pH 6.9 while stirring at 400 rpm. The electrodes were treated in chronoamperometric mode at +1.0 V for 120 s in the same solution and conditions[44]. 17-OHP-GDH

was immobilized on the graphene nanosheets modified surface by first treating the electrode surface with PEI water solution (20 mg $ml^{-1}$) for 1.5 h while moderately shaking. The PEI-functionalized electrodes were rigorously washed twice with 25 mM HEPES pH 7.6. Subsequently, the electrodes were incubated for 2 h with slow shaking in the dark in a solution of 50 mM EDC, 50 mM NHS, 1 µM 17-OHP-GDH and 25 mM HEPES, pH 7.6. The formed bioelectrodes were washed out twice with 25 mM HEPES pH 7.6 before usage. The bioelectrodes were analyzed by cyclic voltammetry scanned at a rate of 5 mV $s^{-1}$ versus the Ag/AgCl/3 M KCl reference.

### Electrode characterization

The constructed bioelectrodes were shown to provide the maximal output at saturating substrate concentration ($I_{max}$) of 22.5 ± 0.01 µA with a limit of detection (3$\sigma$) below 0.5 nM. We determined the apparent Michaelis–Menten constant for 17-OHP ($K_m^{app}$) as 34.5 ± 0.01 nM. The biosensor sensitivity was determined as 4583 µA $mM^{-1}$ $cm^{-2}$ calculated from the slope taken of the linear phase of the binding curve (330 ± 40 µA $mM^{-1}$) divided by electrode working surface area (6 × 6 mm (both sides) = 0.072 $cm^2$).

### Scanning electron microscopy of electrodes

The scanning electron microscopy (SEM) imaging of bioelectrode surfaces was conducted using a JSM 7900F field-emission SEM instrument (JEOL). Before SEM analysis, the electrode was treated with liquid nitrogen and freeze-dried overnight. The freeze-dried electrode surface was then fixed by a Butvar solution B-98 (Sigma) in 1.5% chloroform. The applied accelerator voltage was 5.0 kV with magnification ranges from ×3,000 to ×10,000.

### HDX–MS of biosensor proteins

HDX was performed using fully automated, millisecond HDX labeling and automated online quench-flow fast HDX instrument, ms2min (Applied Photophysics, part of Nicoya Lifesciences), connected to an HDX manager (Waters) directly coupled to a Synapt G2-si mass spectrometer (Waters). Next, 10 µl of apo protein (10 µM) or protein equilibrated with 20 µM 17-OHP (1:2 molar ratio) in formulation buffer (20 mM Tris-HCl and 100 mM NaCl, pH 7.20) was mixed with deuterated labeling buffer (20 mM Tris-HCl, 100 mM NaCl, $pH_{read}$ 6.79, pD 7.20) in a 1:20 ratio at 23 °C to initiate HDX, incubated for mixing times of 100–100 000 ms, then mixed with quench buffer (1 M glycine and 3 M urea, pH 2.45) in a 1:1 ratio at 0 °C and automatically injected into the two-dimensional liquid chromatography–MS system. The sample was digested with an Enzymate pepsin column (Waters), the derived peptides trapped on a VanGuard ACQUITY BEH C18 column (2.1 × 5 mm; Waters) for 3 min at 125 µl $min^{-1}$ and separated on an ACQUITY BEH 1.7-µm C18 column (1 × 100 mm; Waters) with a 7-min linear gradient of acetonitrile (5–40%) supplemented with 0.1% formic acid. Mass spectra were acquired in positive ion resolution mode with ion mobility from 300 to 2,000 *m/z*. The ProteinLynx Global Server 2.5.1 (Waters) was used for spectral assignment of $MS^E$ reference data to identify peptides. DynamX 3.0 (Waters) was used to process and assign isotopic distributions of raw data files for HDX experiments. All HDX–MS experiments were performed in triplicate (technical replicates). Statistical analysis was performed by calculating hybrid significance with global significance thresholding and Welch's *t*-test, essentially as previously described[45]. Structural models were made using ICM 3.9-4 (Molsoft).

### MD simulations

Amber22 was used for all MD simulations[46]. Construction of chimera's structures for the simulations is described above. Hydrogens were added to 17-OHP in the holo structure and 17-OPH was deleted to provide the apo structure for molecule dynamics. 17-OHP was parameterized with the GAFF2 force field with Mulliken charges using the Antechamber module of Amber22 (ref. 47). All simulations were performed in triplicate using the Generalized Born (GB-Neck2) implicit solvent model (igb = 5). Initial energy minimizations entailed 25,000 steps of steepest descent and 25,000 of conjugate gradient with default gradient cutoffs, using random seeds and no positional restraints. These were followed by 2.2 µs of MD simulation collected in batches of 100 ns for each replicate at 300 K using 2-fs timesteps and SHAKE constraints. Frames were collected every 5,000 timesteps and the first 100 ns of each trajectory was discarded, providing production trajectories of 210,000 frames (2.1 µs) for each replicate.

### Use of AI manuscript writing

Generative AI was used at the final stages of manuscript preparation for editing parts of the manuscripts for length and clarity. All changes were verified by the corresponding author.

## Online content

Any methods, additional references, Nature Portfolio reporting summaries, source data, extended data, supplementary information, acknowledgements, peer review information; details of author contributions and competing interests; and statements of data and code availability are available at https://doi.org/10.1038/s41587-026-03081-9.

## References


1. Fenton, A. W. Allostery: an illustrated definition for the 'second secret of life'. *Trends Biochem. Sci.* **33**, 420–425 (2008).
2. Chai, F., Cheng, D., Nasu, Y., Terai, T. & Campbell, R. E. Maximizing the performance of protein-based fluorescent biosensors. *Biochem. Soc. Trans.* **51**, 1585–1595 (2023).
3. Jackson, C., Anderson, A. & Alexandrov, K. The present and the future of protein biosensor engineering. *Curr. Opin. Struct. Biol.* **75**, 102424 (2022).
4. Alberstein, R. G., Guo, A. B. & Kortemme, T. Design principles of protein switches. *Curr. Opin. Struct. Biol.* **72**, 71–78 (2022).
5. Chen, Z. et al. A synthetic protein-level neural network in mammalian cells. *Science* **386**, 1243–1250 (2024).
6. Campbell, E. et al. Chimeric protein switch biosensors. *Adv. Biochem. Eng. Biotechnol.* **187**, 1–35 (2024).
7. Tsao, K. K. et al. The best of both worlds: chemigenetic fluorescent sensors for biological imaging. *Cell Chem. Biol.* **31**, 1652–1664 (2024).
8. Ergun Ayva, C. et al. Exploring performance parameters of artificial allosteric protein switches. *J. Mol. Biol.* **434**, 167678 (2022).
9. Clark, J. J., Benson, M. L., Smith, R. D. & Carlson, H. A. Inherent versus induced protein flexibility: comparisons within and between apo and holo structures. *PLoS Comput. Biol.* **15**, 1–21 (2019).
10. Cooper, A. & Dryden, D. T. F. Allostery without conformational change. *Eur. Biophys. J.* **11**, 103–109 (1984).
11. Wankowicz, S. A. & Fraser, J. S. Advances in uncovering the mechanisms of macromolecular conformational entropy. *Nat. Chem. Biol.* **21**, 623–634 (2025).
12. Choi, J. H., Laurent, A. H., Hilser, V. J. & Ostermeier, M. Design of protein switches based on an ensemble model of allostery. *Nat. Commun.* **6**, 6968 (2015).
13. Barkovskiy, M., Ilyukhina, E., Dauner, M., Eichinger, A. & Skerra, A. An engineered lipocalin that tightly complexes the plant poison colchicine for use as antidote and in bioanalytical applications. *Biol. Chem.* **400**, 351–366 (2019).
14. Jerschke, E., Eichinger, A. & Skerra, A. Drastic alterations in the loop structure around colchicine upon complex formation with an engineered lipocalin indicate a conformational selection mechanism. *Acta Crystallogr. F Struct. Biol. Commun.* **79**, 231–239 (2023).

15. Watson, J. L. et al. De novo design of protein structure and function with RFdiffusion. *Nature* **620**, 1089–1100 (2023).
16. Listov, D., Goverde, C. A., Correia, B. E. & Fleishman, S. J. Opportunities and challenges in design and optimization of protein function. *Nat. Rev. Mol. Cell Biol.* **25**, 639–653 (2024).
17. Lee, G. R. et al. Small-molecule binding and sensing with a designed protein family. *Nat. Commun.* https://doi.org/10.1038/s41467-026-70953-8 (2026).
18. Wu, K. et al. Design of intrinsically disordered region binding proteins. *Science* **389**, eadr8063 (2025).
19. Liu, C. et al. Diffusing protein binders to intrinsically disordered proteins. *Nature* **644**, 809–817 (2025).
20. Vázquez Torres, S. et al. De novo design of high-affinity binders of bioactive helical peptides. *Nature* **626**, 435–442 (2024).
21. Guo, Z. et al. Development of epistatic YES and AND protein logic gates and their assembly into signalling cascades. *Nat. Nanotechnol.* **18**, 1327–1334 (2023).
22. Guo, Z. et al. Lanthanide-controlled protein switches: development and in vitro and in vivo applications. *Angew. Chem. Int. Ed. Engl.* **64**, e202411584 (2025).
23. Oubrie, A. Structure and mechanism of soluble glucose dehydrogenase and other PQQ-dependent enzymes. *Biochim. Biophys. Acta* **1647**, 143–151 (2003).
24. Hall, M. P. et al. Engineered luciferase reporter from a deep sea shrimp utilizing a novel imidazopyrazinone substrate. *ACS Chem. Biol.* **7**, 1848–1857 (2012).
25. Yeh, A. H.-W. et al. De novo design of luciferases using deep learning. *Nature* **614**, 774–780 (2023).
26. Vergara, R. et al. LuxSit Pro and sPro: next-generation designed luciferases for bioluminescent reporting and complementation-based detection. Preprint at *bioRxiv* https://doi.org/10.1101/2025.07.21.665742 (2025).
27. Meister, G. E. & Joshi, N. S. An engineered calmodulin-based allosteric switch for peptide biosensing. *ChemBioChem* **14**, 1460–1467 (2013).
28. Guo, Z. et al. Generalizable protein biosensors based on synthetic switch modules. *J. Am. Chem. Soc.* **141**, 8128–8135 (2019).
29. Orton, H. W. et al. Through-space scalar $^{19}F$–$^{19}F$ couplings between fluorinated noncanonical amino acids for the detection of specific contacts in proteins. *J. Am. Chem. Soc.* **143**, 19587–19598 (2021).
30. Kish, M., Ivory, D. P. & Phillips, J. J. Transient structural dynamics of glycogen phosphorylase from nonequilibrium hydrogen/deuterium-exchange mass spectrometry. *J. Am. Chem. Soc.* **146**, 298–307 (2024).
31. Smit, J. H. et al. Probing universal protein dynamics using hydrogen–deuterium exchange mass spectrometry-derived residue-level Gibbs free energy. *Anal. Chem.* **93**, 12840–12847 (2021).
32. Mutschler, R. et al. Cooperative binding domains enhance sensitivity and over-come the hook effect in two-component protein biosensors. *ACS Sens.* https://doi.org/10.1021/acssensors.6c00488 (2026).
33. Nicholes, N. et al. Modular protein switches derived from antibody mimetic proteins. *Protein Eng. Des. Sel.* **29**, 77–85 (2016).
34. Zou, Y. et al. Minimally invasive electrochemical continuous glucose monitoring sensors: recent progress and perspective. *Biosens. Bioelectron.* **225**, 115103 (2023).
35. Nasu, Y., Shen, Y., Kramer, L. & Campbell, R. E. Structure- and mechanism-guided design of single fluorescent protein-based biosensors. *Nat. Chem. Biol.* **17**, 509–518 (2021).
36. Guntas, G., Mansell, T. J., Kim, J. R. & Ostermeier, M. Directed evolution of protein switches and their application to the creation of ligand-binding proteins. *Proc. Natl Acad. Sci. USA* **102**, 11224–11229 (2005).
37. Buller, A. R. et al. Directed evolution mimics allosteric activation by stepwise tuning of the conformational ensemble. *J. Am. Chem. Soc.* **140**, 7256–7266 (2018).
38. Wait, S. J. et al. Machine learning-guided engineering of genetically encoded fluorescent calcium indicators. *Nat. Comput. Sci.* **4**, 224–236 (2024).
39. Ghavami, A. et al. Assay for drug discovery: synthesis and testing of nitrocefin analogues for use as β-lactamase substrates. *Anal. Biochem.* **486**, 75–77 (2015).
40. Mukai, T. et al. Highly reproductive *Escherichia coli* cells with no specific assignment to the UAG codon. *Sci. Rep.* **5**, 9699 (2015).
41. Dauparas, J. et al. Atomic context-conditioned protein sequence design using LigandMPNN. *Nat. Methods* **22**, 717–723 (2025).
42. Wu, K. et al. Design of intrinsically disordered region binding proteins. **389**, eadr8063 (2025).
43. Dauparas, J. et al. Robust deep learning-based protein sequence design using ProteinMPNN. *Science* **378**, 49–56 (2022).
44. Gamella, M., Guo, Z., Alexandrov, K. & Katz, E. Bioelectrocatalytic electrodes modified with PQQ-glucose dehydrogenase–calmodulin chimera switchable by peptide signals: pathway to generic bioelectronic systems controlled by biomolecular inputs. *ChemElectroChem* **6**, 638–645 (2019).
45. Seetaloo, N., Kish, M. & Phillips, J. J. Software for flexible high structural resolution of hydrogen/deuterium-exchange mass spectrometry data. *Anal. Chem.* **94**, 4557–4564 (2022).
46. Case, D. A. et al. AmberTools. *J. Chem. Inf. Model.* **63**, 6183–6191 (2023).
47. He, X., Man, V. H., Yang, W., Lee, T.-S. & Wang, J. A fast and high-quality charge model for the next generation general AMBER force field. *J. Chem. Phys.* **153**, 114502 (2020).
48. Qianzhu, H. $^{19}F$-NMR spectra of artificial 17-OPH biosensor (cpOHPFA_1952-20-BLA-253) in apo and holo states. *Zenodo* https://doi.org/10.5281/zenodo.18383997 (2026).

### Reporting summary

Further information on research design is available in the Nature Portfolio Reporting Summary linked to this article.

## Data availability

The HDX–MS data were deposited to the ProteomeXchange Consortium through the PRIDE partner repository with the dataset identifier PXD073666. The $^{19}$F-NMR spectra were deposited to Zenodo (https://doi.org/10.5281/zenodo.18383997)[48]. The data supporting the findings of this study are available in the paper and its Supplementary Information. Source data are provided with this paper.

## Acknowledgements

This work was supported by Australian Research Council grants DP160100973, LP200200916 and CE200100029 to K.A., CE200100012 to C.J.J. and G.O., and DP230100079 and DP240100273 to T.H. and G.O. The work was also supported by National Health and Medical Research Council grant APP 2033951 to K.A. K.A. and Z.C. were supported by CSIRO SybBio and Advanced Engineering Biology Future Science Platform. M.K. and J.J.P. were supported by UK Research Institute Future Leaders fellowship MR/T02223X/1 and MR/Z000157. E.K. and O.S. were supported by the National Science Foundation grant CBET-2235349 including IMPRESS-U supplement and NSF-BSF CBET-2422672. G.R.L., D.B. and K.W. acknowledge funding from Open Philanthropy Project Improving Protein Design Fund Innovation Fellows Program and Howard Hughes Medical Institute. K.A. acknowledges support from the QUT Centre for Agriculture and the Bioeconomy. We thank Monod Bio, Inc. for providing reagents for the LuxSit Pro assays, and we thank S. Fleishman, A. Skerra and I. Berezovsky for insightful discussions and suggestions on the manuscript and R. Abagyan for expert advice on data visualization.

## Author contributions

Z.G., O.S., M.K., J.J.P., G.R.L. and H.Q. designed and performed the experiments, analyzed the data and wrote the manuscript. C.J.J., G.O., M.M.F., O.S., A.Q.R., E.K., A.C.W. and T.H. designed the experiments, analyzed the data and wrote the manuscript. R.M. designed and performed the experiments. D.B. and K.W. designed the experiments and analyzed the data. K.A. secured funding, managed the project, designed the experiments, analyzed the data and wrote the manuscript.

## Competing interests

Z.G. and K.A. are named inventors on patent applications covering YES-gate biosensor technology and biosensors with auxiliary binding domains either used or described in this study. K.A. holds shares in CIDER Biotech that holds a license for these technologies. The remaining authors declare no competing interests.

## Additional information

**Supplementary information** The online version contains supplementary material available at https://doi.org/10.1038/s41587-026-03081-9.

**Correspondence and requests for materials** should be addressed to Kirill Alexandrov.

**Peer review information** *Nature Biotechnology* thanks Sahika Inal and the other, anonymous, reviewer(s) for their contribution to the peer review of this work. Peer reviewer reports are available.

nature portfolio

Corresponding author(s): Kirill Alexandrov

Last updated by author(s): Feb 21, 2026

# Reporting Summary

Nature Portfolio wishes to improve the reproducibility of the work that we publish. This form provides structure for consistency and transparency in reporting. For further information on Nature Portfolio policies, see our Editorial Policies and the Editorial Policy Checklist.

## Statistics

For all statistical analyses, confirm that the following items are present in the figure legend, table legend, main text, or Methods section.

| n/a | Confirmed |
|---|---|
| ☐ | ☒ The exact sample size (*n*) for each experimental group/condition, given as a discrete number and unit of measurement |
| ☐ | ☒ A statement on whether measurements were taken from distinct samples or whether the same sample was measured repeatedly |
| ☒ | ☐ The statistical test(s) used AND whether they are one- or two-sided<br>*Only common tests should be described solely by name; describe more complex techniques in the Methods section.* |
| ☒ | ☐ A description of all covariates tested |
| ☒ | ☐ A description of any assumptions or corrections, such as tests of normality and adjustment for multiple comparisons |
| ☐ | ☒ A full description of the statistical parameters including central tendency (e.g. means) or other basic estimates (e.g. regression coefficient) AND variation (e.g. standard deviation) or associated estimates of uncertainty (e.g. confidence intervals) |
| ☒ | ☐ For null hypothesis testing, the test statistic (e.g. *F*, *t*, *r*) with confidence intervals, effect sizes, degrees of freedom and *P* value noted<br>*Give P values as exact values whenever suitable.* |
| ☒ | ☐ For Bayesian analysis, information on the choice of priors and Markov chain Monte Carlo settings |
| ☒ | ☐ For hierarchical and complex designs, identification of the appropriate level for tests and full reporting of outcomes |
| ☒ | ☐ Estimates of effect sizes (e.g. Cohen's *d*, Pearson's *r*), indicating how they were calculated |

*Our web collection on statistics for biologists contains articles on many of the points above.*

## Software and code

Policy information about availability of computer code

| | |
|---|---|
| Data collection | b-lactamase and GDH absorption assays - Cary WinUV Software, Electrochemical measurements- GPES 4.9 software, NanoLuc and LuxSit Pro luminescent measurements Tecan plate reader . HDX-MS -Masslynx v4.1 SCN957 (Waters) |
| Data analysis | Protein Lynx Global Server v3.0.3 (Waters); DynamX v3.0 (Waters); Matlab R2019a (Mathworks); Pymol 2.3.5 (Schrodinger); Prism v8 (Graphpad), Grafit 5.0, MassLynx v4.1 SCN 957 (Waters) |

For manuscripts utilizing custom algorithms or software that are central to the research but not yet described in published literature, software must be made available to editors and reviewers. We strongly encourage code deposition in a community repository (e.g. GitHub). See the Nature Portfolio guidelines for submitting code & software for further information.

## Data

Policy information about availability of data

All manuscripts must include a data availability statement. This statement should provide the following information, where applicable:

- Accession codes, unique identifiers, or web links for publicly available datasets
- A description of any restrictions on data availability
- For clinical datasets or third party data, please ensure that the statement adheres to our policy

The authors declare that the data supporting the findings of this study are available in this paper, ts supplementary information files or has been uploaded in public repositories . Assess codes for all PDB entries analyzed are included in the manuscript.

# Field-specific reporting

Please select the one below that is the best fit for your research. If you are not sure, read the appropriate sections before making your selection.

☒ Life sciences ☐ Behavioural & social sciences ☐ Ecological, evolutionary & environmental sciences

For a reference copy of the document with all sections, see nature.com/documents/nr-reporting-summary-flat.pdf

# Life sciences study design

All studies must disclose on these points even when the disclosure is negative.

| | |
|---|---|
| Sample size | N/A |
| Data exclusions | no data was excluded from analysis |
| Replication | the replicates confirmed the observed effects, experiments were performed in parallel triplicates |
| Randomization | randomization was not relevant to this study |
| Blinding | *Describe whether the investigators were blinded to group allocation during data collection and/or analysis. If blinding was not possible, describe why OR explain why blinding was not relevant to your study.* |

# Reporting for specific materials, systems and methods

We require information from authors about some types of materials, experimental systems and methods used in many studies. Here, indicate whether each material, system or method listed is relevant to your study. If you are not sure if a list item applies to your research, read the appropriate section before selecting a response.

## Materials & experimental systems

| n/a | Involved in the study |
|---|---|
| ☒ | ☐ Antibodies |
| ☒ | ☐ Eukaryotic cell lines |
| ☒ | ☐ Palaeontology and archaeology |
| ☒ | ☐ Animals and other organisms |
| ☒ | ☐ Human research participants |
| ☒ | ☐ Clinical data |
| ☒ | ☐ Dual use research of concern |

## Methods

| n/a | Involved in the study |
|---|---|
| ☒ | ☐ ChIP-seq |
| ☒ | ☐ Flow cytometry |
| ☒ | ☐ MRI-based neuroimaging |